Available online at www.sciencedirect.com
ScienceDirect
Acta Materialia 55 (2007) 1309–1318
Acta MATERIALIA
www.actamat-journals.com

Pin-on-disk wear behavior in a like-on-like configuration in a biological environment of high carbon cast and low carbon forged Co–29Cr–6Mo alloys

Akihiko Chiba [a,*], Kazushige Kumagai [b], Naoyuki Nomura [a], Satoru Miyakawa [b]

[a] Department of Welfare Engineering, Faculty of Engineering, Iwate University, 4-3-5 Ueda, Morioka 020-8551, Japan
[b] Iwate University, 4-3-5 Ueda, Morioka 020-8551, Japan

Received 17 May 2006; received in revised form 17 September 2006; accepted 2 October 2006
Available online 8 December 2006

Abstract

In order to examine the effects of carbides and microstructures on the wear behavior of a biomedical Co–Cr–Mo alloy in Hanks solution, the wear behavior of a forged Co–Cr–Mo alloy without addition of Ni and C (hereafter designated the forged CoCr alloy) and a high carbon cast CoCr alloy (hereafter designated the cast CoCr alloy) sliding against themselves have been investigated using a pin-on-disk type wear testing machine. The wear loss of the forged CoCr alloy was found to be much smaller than that of the cast CoCr alloy. Carbide precipitation in the coarse-grained structure of the cast CoCr alloy would account for the higher abrasive wear loss. The forged CoCr alloy, with no carbide and a refined grain size, which is more prone to strain-induced martensitic transformation, would exhibit excellent like-on-like wear resistance, mostly against surface fatigue wear, compared to the carbide-hardened cast CoCr alloy.

Keywords: Biomaterials; Cobalt alloys; Wear; Martensitic phase transformation; Forging

1. Introduction

Cobalt chromium molybdenum (cobalt chrome or CoCr) alloys are widely used as implant materials in such applications as hip and knee prostheses due to their excellent corrosion and wear resistance, as well as their good mechanical properties [1–4]. Today, the most widely accepted combination of bearing materials for the hip joint consists of a femoral head fabricated from CoCr alloy articulating against a polymeric component made of ultrahigh molecular weight polyethylene (UHMWPE). Although the use of the CoCr/UHMWPE bearing couple has provided consistent results in total hip arthroplasties, wear of the UHMWPE component is a major obstacle limiting the longevity of these reconstructions. It is now well established that UHMWPE particulate wear debris generated from the articulating surfaces initiates a cascade of adverse tissue response leading to osteolysis and in certain cases loosening of the components [5]. Extending the longevity of total joint replacements using alternative bearing technologies with improved wear behavior has been the subject of ongoing research in the orthopaedic community. Through efforts to modify the tribological characteristics of UHMWPE, crosslinking of the UHMWPE is revealed to substantially improve the wear performance of the material in hip joint simulators [6]. Another approach to the problem caused by UHMWPE wear particles has been to use alternative bearing surfaces such as metal-on-metal (MOM) articulation, intended to significantly reduce or minimize wear at the articulating surface, thereby reducing the risk of debris-mediated bone loss and aseptic loosening. It was previously reported that mean wear rates of second-generation and first-generation MOM hip prostheses were as low as 0.3 and 1–6 mm^3 per year [7], respectively,

* Corresponding author. Tel./fax: +81 19 621 6349.
E-mail address: a.chiba@iwate-u.ac.jp (A. Chiba).

1359-6454/$30.00
doi:10.1016/j.actamat.2006.10.005

compared to 30–100 mm^3 for traditional metal-on-UHMWPE hip joints [8].

Although a low wear volume is not in itself the only important factor governing the long-term clinical outcome of a total hip replacement (THR), MOM bearings are showing considerable potential as an osteolysis-free THR. Thus there is renewed interest in MOM bearings as a solution to this problem in view of their potential for greatly improved wear performance. However, MOM wear tests have demonstrated varying results, depending on the carbon content of the alloy and whether or not it was heat treated. For instance, Medley et al. [9,10] reported on the basis of their study on the wear behavior of the MOM bearing couples using a hip simulator that a low carbon forged CoCrMo alloy has lower wear than either a high carbon cast alloy or low carbon commercial alloy. In contrast, there exist a number of reports [11,12] suggesting that high carbon forged CoCrMo may possess superior wear performance because of the presence of small, finely-distributed carbides at the surface rather than the coarse, more widely-spaced surface carbides of the cast alloy. As to improvement in wear resistance of MOM bearings comprising CoCrMo alloys, previous research suggests that there are at least two possibilities for manufacturing CoCr/CoCr MOM bearing couples with the greatest wear resistance; one is the couple of low carbon forged CoCrMo with itself and the other is high carbon forged CoCrMo with itself. Research on the former couple has revealed a close relationship between grain size and wear resistance and for that reason, recrystallized CoCrMo specimens with various fine grain sizes are required. However, obtaining such specimens is difficult because the CoCrMo alloy has limited ductility without addition of carbon and Ni, so that heavily plastic deformation of the CoCrMo alloy at elevated temperatures is of limited utility in controlling the microstructure. A further point to note is that study of high carbon CoCrMo alloy is rendered problematic because of difficulties in controlling the grain size as well as the distribution, size and/or morphology of the carbide precipitation.

In a previous study [3], we have successfully fabricated a CoCrMo alloy containing no Ni and C, with fine grain sizes by using a thermomechanical technique and revealed its mechanical properties such as tensile strength, ductility and dry wear behavior [13]. Thus the present study is a preliminary investigation to establish the microstructure of the CoCrMo alloy most suitable for MOM bearings. For this purpose, the aim of the present investigation is to compare the wear behavior of like-on-like pairings of the forged CoCrMo alloy with fine-grained structure and without carbon addition with a high carbon commercial cast CoCrMo alloy (standardized ASTM F75).

2. Experimental

A cast CoCr alloy with composition in accordance with ASTM F-75 98 (ISO 5832-4: 1996) was purchased from a supplier and used as received (hereafter designated the “cast CoCr alloy”). In order to obtain a forged CoCr alloy, a vacuum induction melting technique was employed to prepare a Co–Cr–Mo alloy ingot of $\sim$5 kg with a diameter of $\sim$80 mm at the top and 70 mm at the bottom and a length of 130 mm. Prior to forging, the ingot underwent annealing treatment for 12 h at 1523 K for homogenization and then it was cooled in water. The ingot was forged at temperatures $\gtrsim$ 1273 K; the forging temperature of >1273 K was carefully maintained during forging to prevent phase transformation from the fcc-Co phase (γ phase), which is stable at temperatures $\gtrsim$ 1273 K, to the hcp-Co phase (ε phase), which has limited ductility due to a shortage of the independent slip system, according to von Mises criteria. The ingot was forged in reduction by $\sim$45% and subsequently clad-forged with a stainless steel pipe into a plate of thickness $\sim$8 mm and width $\sim$77 mm. Through these processes, we obtained the “forged CoCr alloy” with an overall reduction in area of $\sim$82%. The nominal and chemical compositions of the cast CoCr alloy and the forged CoCr alloy are listed in Table 1.

2.1. Microstructural characterization

Each specimen was examined metallographically to identify the microstructure and grain size. Sample preparation for optical microscope (OM) observation was done by polishing with 200–1200 emery paper and then electropolishing at a voltage of 6 V and a temperature of 273 K in a solution of 90 parts methanol plus five parts sulfuric acid. Transmission electron microscope (TEM) observations were conducted for identification of microstructures in the cast and forged CoCr alloys. Discs of thickness $\sim$1 mm were made from each alloy using a wire-cut spark machine and mechanically polished with emery paper to a thickness of $\sim$0.1 mm. Thin foils for TEM observations were prepared by jet-electropolishing the disc at a voltage of 12 V and a temperature of 243 K in a solution of 90 parts methanol plus five parts sulphuric acid. TEM (Hitachi H-800) observations were performed (at an accelerated voltage of 200 kV).

Crystal structures and identification of second phase precipitates for both the alloys were determined with an X-ray diffractometer (XRD) using monochromated Cu Kα radiation over $20^\circ \leqslant 2\theta \leqslant 100^\circ$. The diffraction experiments were also used for determining integrated intensities for the most intense isolated $\gamma\{200\}$ and $\varepsilon\{10\bar{1}1\}$ X-ray

Table 1
Chemical composition (mass %) of ingots obtained in the present study, together with the chemical requirements of ASTM F75

Ingot	Co	Cr	Mo	Ni	C	Si	O	N
ASTM F75	Bal.	28.45	6.06	0.16	0.26	–	0.0028	0.0018
Forged CoCr	Bal.	28.42	5.92	<0.01	0.067	<0.01	0.0032	0.0006

diffraction peaks. Quantitative analyses of the volume fractions of fcc-γ and hcp-ε phases were carried out using the method proposed by Sage and Guillaud [14]. The volume fractions were calculated as follows:

$$\frac{x}{1-x} = \frac{1}{4} \times \frac{1.85}{0.27} \times \frac{I_{(200)\gamma}}{I_{(10\bar{1}1)\varepsilon}} \quad (1)$$

where x is the volume fraction of γ phase and $I(200)_\gamma$ and $I(10\bar{1}1)_\varepsilon$ are the integrated intensities of the $(200)_\gamma$ and $(10\bar{1}1)_\varepsilon$ peaks, respectively.

Wear scars were also analyzed with an electron probe microanalyzer (EPMA) and micro-area XRD using Cr Kα radiation with a collimator of 100 μm in diameter. The XRD profiles from wear scars were collected at three different positions and the typical profile was used for analysis.

Hardness of the wear scar was evaluated by a micro Vickers hardness tester at a load of 9.8 N and compared with that of the as-polished (unworn) specimen.

2.2. Pin-on-disk wear tests

The disk specimens for wear tests were cut from the cast CoCr alloy bar and the forged CoCr alloy plate with a wire-cut spark machine. The disk specimens were 30 mm in diameter and 5 mm in thickness. The pin samples were machined from the cast CoCr bar and the forged CoCr alloy plate in the form of pins of diameter 6 mm and length 20 mm. In order to maintain a contact stress of 3.12 MPa, the pin heads were machined into flats of 2 mm in diameter. The surfaces of disk specimens and the pin heads were polished with SiC paper to 1000 grit. Final polishing was carried out with alumina suspensions of 1, 0.3 and 0.05 μm and then with a silica suspension with 10% H_2O_2. Thereafter, the disks and the pin were subjected to a surface roughness test to ensure that the surface roughness (R_a) was <0.05 μm. Roughness measurements were conducted using a Taylor Hobson Form Talysurf PGI 1240.

Wear tests were carried out three times for each specimen ($n = 3$) on a conventional pin-on-disk apparatus (RHSCA FRP-2000). The test lubricant used was Hanks solution heated to 37 °C. The pins were uniformly loaded on alloy disks with a constant load of 9.8 N corresponding to a contact stress of 3.12 MPa. The disk rotating speed was ∼24 rpm (20 mm/s). The main track radius for pins was 8 mm. Each experiment was run for a total of 7 days (1.21×10^7 mm sliding distance) with the machine stopped every 6 h for measurement of wear. Prior to weighing, the pins and disks were cleaned ultrasonically with 100% acetone for ∼5 min. The wear volumes of the pins and disks were determined gravimetrically after each test period. The progressive gravimetric wear of both specimens tested was converted to volumetric values (using a density for the forged and cast CoCr alloys of 8.41 and 8.37 mg/mm^3, respectively; densities were measured by Archimedes method). The wear volume V and wear factor ω_s of the discs were calculated as follows:

$$V = \frac{M_{\mathrm{loss}}}{\rho} \quad (2)$$

$$\omega_s = \frac{M_{\mathrm{loss}}}{W \times L \times \rho} \quad (3)$$

where M_{loss} is the weight loss of the disc, L the sliding distance, W the contact load and ρ the density of the disk.

3. Results and discussion

3.1. Microstructure characterization

Optical microstructures of the both alloys are illustrated in Fig. 1a and b. The cast CoCr (Fig. 1a) exhibits a coarse dendritic structure with an interdendritic phase of $M_{23}C_6$-type carbide, which is characteristic of investment casting of an ASTM F-75 alloy. The microstructure of the forged CoCr alloy (Fig. 1b) shows no carbides and consists of an equiaxed and fine-grained structure with an average grain size of ∼11 μm. A TEM micrograph of the forged CoCr alloy is shown in Fig. 2. This also shows equiaxed grains

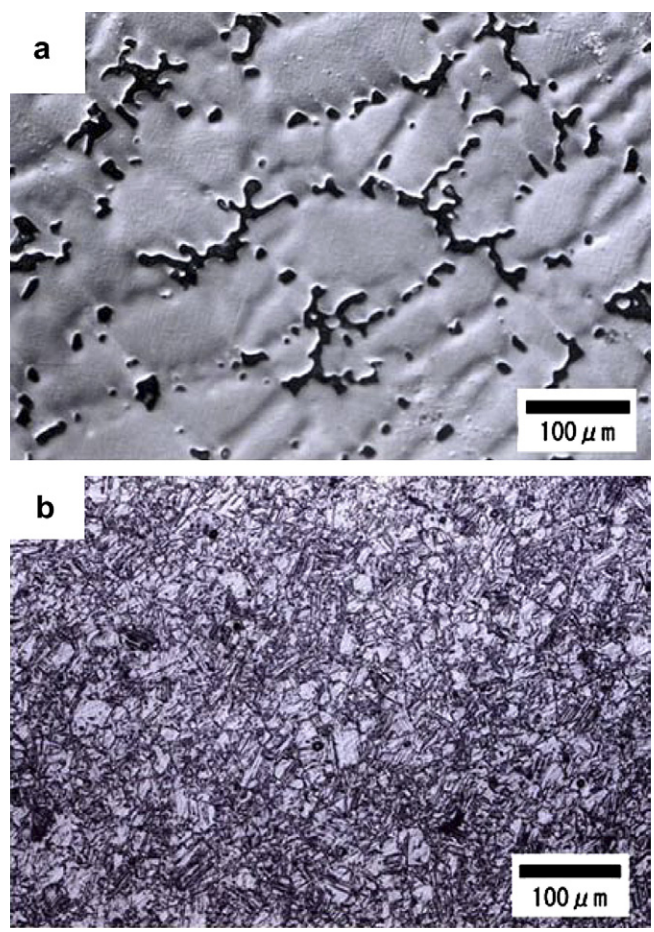

Fig. 1. Optical microstructure of: (a) the cast CoCr alloy and (b) the forged CoCr alloy.

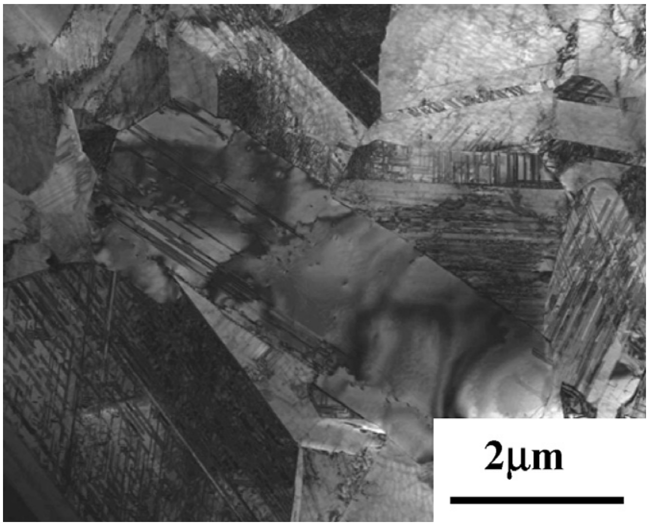

Fig. 2. TEM micrograph of the forged CoCr alloy.

with a profusion of the stacking faults and fine bands of the ε martensitic phase. No carbide precipitation was found in this TEM observation.

XRD patterns of the cast CoCr alloy and the forged CoCr alloy are shown in Fig. 3a and b, respectively. In each figure the diffraction patterns at upper and lower positions are taken from the wear scar and the unworn disc surfaces, respectively. A comparison of these XRD patterns shows that in the cast CoCr alloy (Fig. 3a) an fcc-γ phase (indicated by a solid circle) is mainly observed in the unworn surface, whereas a γ phase and small amount of an hcp-ε phase (indicated by an open circle) appear in the worn surface (i.e., wear scar); the ε phase was formed by a strain-induced martensitic transformation (SIMT) during wear. On the other hand, the XRD pattern taken from the unworn surface of the forged CoCr, indicated in Fig. 3b, consists mainly of γ phase and some slight ε phase; the volume fraction of γ to ε is estimated to be 75% according to Eq. (1). After the wear test, the XRD pattern on the wear scar mainly comprised the peaks from the strain-induced martensitic ε phase, though small peaks from γ phase are still seen in the XRD pattern. Accordingly, it can be concluded from the XRD analyses that the forged CoCr is more prone to martensitic transformation than the cast CoCr alloy. This is because the cast CoCr alloy contains carbon which is effective in raising the stacking fault energy [15], while the forged CoCr alloy has no addition of carbon.

3.2. Wear behavior

3.2.1. Coefficient of friction

Fig. 4 shows the friction coefficient, μ, for the cast CoCr alloy (●) and the forged CoCr alloy (○) as a function of sliding distance. The value of μ for the forged CoCr alloy is almost equivalent to that for the cast CoCr during an initial sliding distance. By increasing the sliding distance we find that the values of μ for the cast CoCr and forged CoCr alloy slightly increase from 0.50 to 0.59 and from 0.54 to 0.63, respectively. Thus it is found that the friction coefficient for a like-on-like pairing of the forged CoCr alloy is slightly higher than that for the cast CoCr alloy. In a previous paper [13], we reported the dry friction and wear properties of a forged Co–29Cr–6Mo alloy sliding against an alumina ball in air and obtained a friction coefficient of 0.34 – almost half the value obtained in the present study which was conducted in a lubricant environment. In general, the friction coefficient μ is thought to be smaller in the lubricant condition than in the dry condition. However,

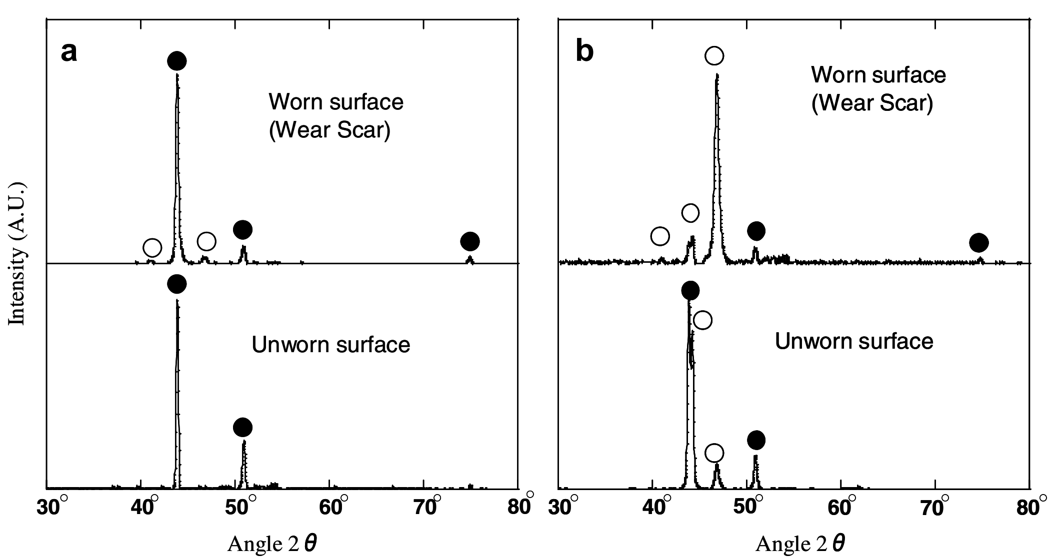

Fig. 3. X-ray diffraction patterns of: (a) the cast CoCr alloy and (b) the forged CoCr alloy. In each figure at the upper and lower positions are shown diffraction patterns taken from the wear scar after the wear tests and the as-polished (unworn) disc surface, respectively. ● peak from fcc-γ phase, ○ peak from hcp-ε phase.

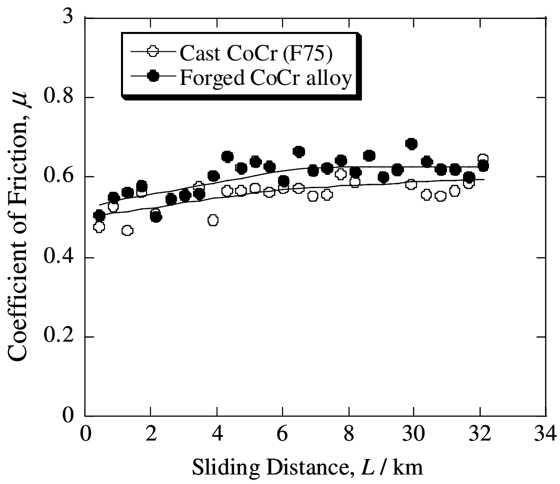

Fig. 4. Coefficient of friction for the cast (●) and forged (○) CoCr alloys as a function of sliding distance.

the values obtained in the present study do not obey this general rule.

3.2.2. Wear volume

Wear volumes for both disks and pins of the cast CoCr alloy and the forged CoCr alloy plotted against the sliding distance are shown in Fig. 5a and b, respectively. Each plot indicated in the figure is the average of three measurements and the vertical bars on each plot connect the maximum and minimum values. The wear volume for the disk of the cast CoCr alloy (Fig. 5a) increased with sliding distance and reached 0.36 mm^3 at the final sliding distance of 12.1 km. The wear volume of the pin initially increased up to a sliding distance of ~3 km and thereafter reached an almost constant value of 0.09 mm^3 until the final sliding distance of 12.1 km was reached. It is to be noted that the wear volume for the disk was noticeably different from that of the pin; the former was four times larger than the latter at the final sliding distance. This may stem from a transfer of the wear debris generated from the surface of the disk to that of the pin during wear. It seems that a characteristic feature of the like-on-like wear behavior of the cast CoCr alloy is a disk–pin asymmetry in wear volume, though causes for that are not clearly understood at present.

The wear volume for the disk of the forged CoCr alloy (Fig. 5b) was barely apparent until a sliding distance of ~4 km was reached and thereafter increased linearly with sliding distance. The final wear volume for the disk of the forged CoCr reached ~0.15 mm^3, which is less than half the value for the disk of the cast CoCr alloy (0.36 mm^3). The wear volume vs. sliding distance for the pin showed a similar tendency to that for the disk in the forged CoCr alloys, and its final wear volume was 0.09 mm^3, which is slightly smaller than that for the disk. Thus it was found that, unlike the cast CoCr alloy, the disk–pin symmetry of the wear volume of the forged CoCr alloy holds relatively true.

Although the plot based on the average values of three measurements is not enough to determine the degree of the scatter, it can give us an outline of the trend of the wear behavior of both alloys. Thus we consider that the length of the vertical bars concomitant with the plots is associated with the reproducibility of the wear process; the greater the length of the vertical bars, the less the reproducibility of the wear process. The length of the vertical bars is greater in the cast CoCr alloy than in the forged CoCr alloy, indicating that the reproducibility of wear process in the forged CoCr alloy is much higher than that in the cast CoCr alloy. It is likely that lack of reproducibility of the wear process stems from the same mechanism as the disk–pin asymmetry observed in wear volume in the cast CoCr alloy shown in Fig. 5a.

3.2.3. Wear factor

On the basis of the relation between wear volume and sliding distance, the wear factors for the cast CoCr alloy and the forged CoCr alloy, calculated from Eq. (2) using

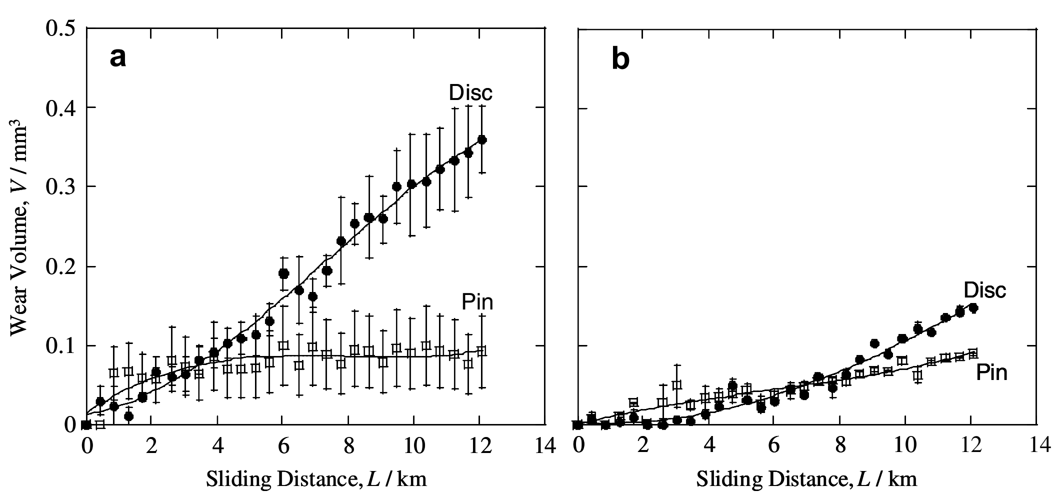

Fig. 5. Wear volume for both disc and pin of: (a) the cast CoCr alloy and (b) the forged CoCr alloy plotted against sliding distance.

average values of the wear volume, are plotted against the sliding distance in Fig. 6a and b, respectively. For the cast CoCr alloy (Fig. 6a), the wear factor of the disk is almost constant, irrespective of sliding distance, showing a value of 3.0×10^{-9} mm^2 N^{-1}. The wear factor of the pin gradually decreases with sliding distance and reaches a value of 7.1×10^{-10} mm^2 N^{-1}. The final wear factor of the disk is quite different from that of the pin, a similar trend to the wear volume shown in Fig. 5a. On the other hand, for the forged CoCr alloy (Fig. 6b), the wear factor for the disk slightly increases with sliding distance, whereas that for the pin slightly decreases with sliding distance. The wear factors for the disk and the pin at the final sliding distance are 1.2×10^{-9} and 7.6×10^{-10} mm^2 N^{-1}, respectively.

The overall wear volume and the overall wear factor, i.e., wear volume and wear factor for disk + pin, are shown in Fig. 7a and b, respectively. The overall wear volumes of the cast CoCr alloy and the forged CoCr alloy (in Fig. 7a) are 0.45 and 0.24 mm^3, respectively, at the final sliding distance. In addition, the overall wear factors of the cast CoCr alloy and the forged CoCr alloy are 3.8 and 2.0×10^{-9} mm^2 N^{-1}, respectively, at the final sliding distance. Thus it is concluded that the wear behavior is more pronounced in the cast CoCr alloy than in the forged CoCr alloy.

3.2.4. Wear appearances

Fig. 8a and b show scanning electron microscope (SEM) micrographs of the wear scars of the cast CoCr alloy and the forged CoCr alloy, respectively, obtained in secondary electron mode (SEI) after 7 days of continuous measurements. Scratches and various grooves parallel to the moving direction of the pin appear in the wear scar. It is to be noted that the number of scratches and the grooves per unit area on the scar are higher in the cast CoCr alloy (Fig. 8a) than in the forged CoCr alloy (Fig. 8b). It is likely that the grooves and the scratches are formed by abrasion with the carbide asperities of the pin and wear debris generated from matrix and torn-off carbides.

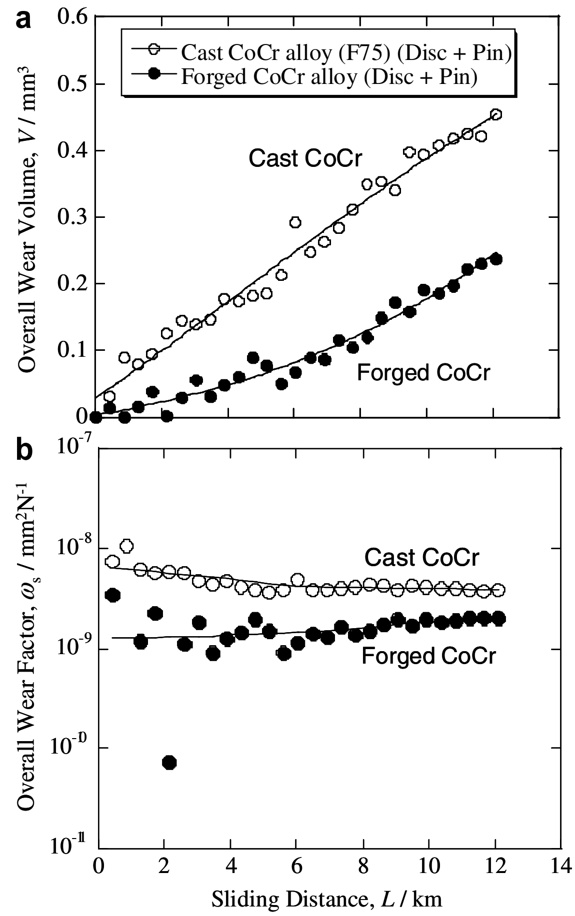

Fig. 7. (a) Overall wear volumes and (b) wear factors of the cast forged CoCr alloys.

Fig. 9 shows an isolated wear scar on the wear surfaces of the cast CoCr alloy: (a) SEM micrograph obtained in secondary electron mode (SEI) and X-ray maps of (b) P,

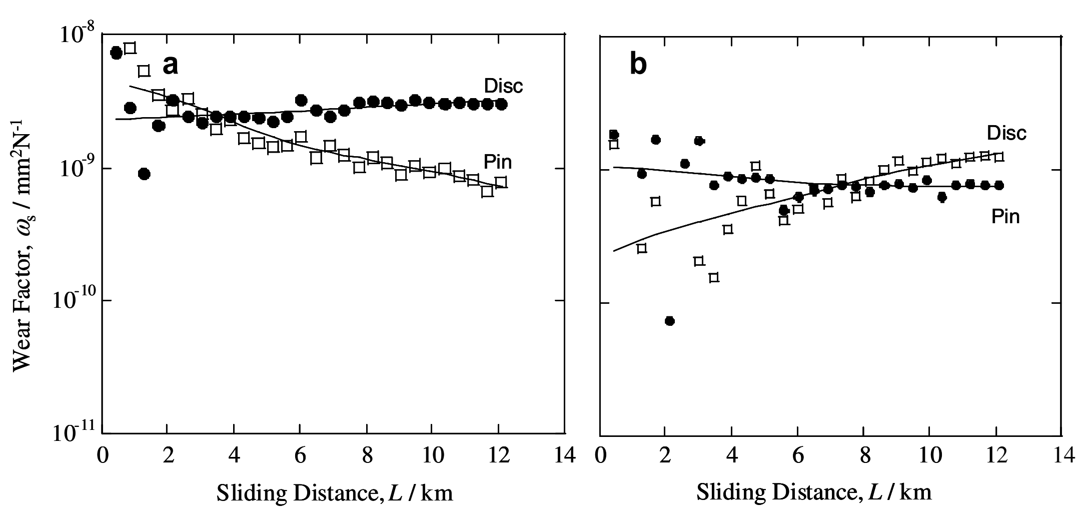

Fig. 6. Wear factors for both disc and pin of: (a) the cast CoCr alloy and (b) the forged CoCr alloy plotted against sliding distance.

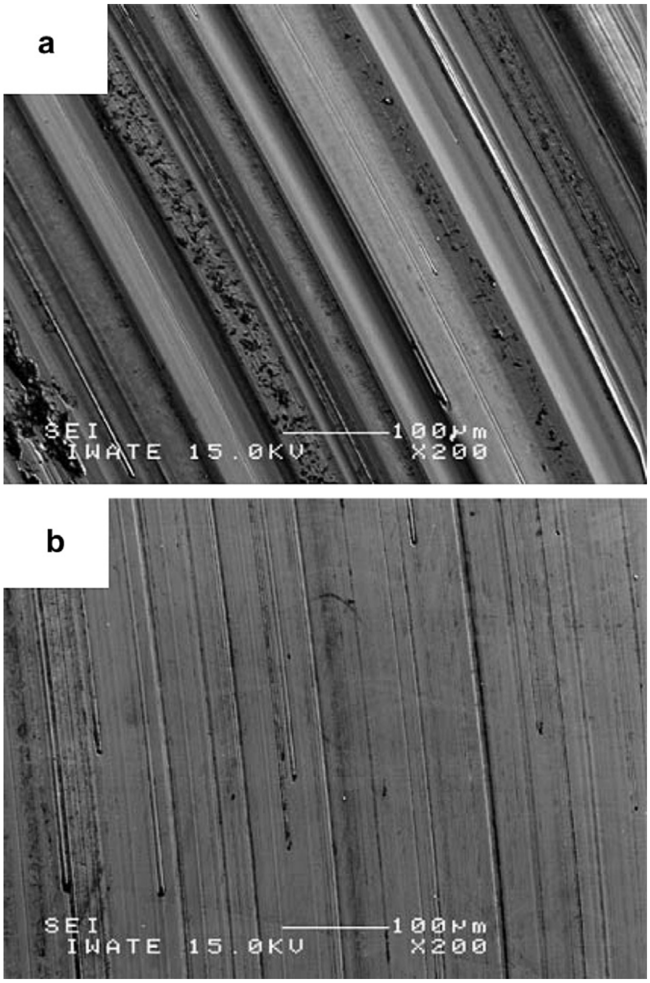

Fig. 8. SEM micrographs obtained in secondary electron mode (SEI) of the wear scars of: (a) the cast CoCr alloy and (b) the forged CoCr alloy. Note that various narrow grooves and scratches are observed in the wear scars.

(c) Ca and (d) O. In Fig. 9a the isolated wear scar seems to be a heavily plastically deformed zone compared to the surroundings. According to the X-ray maps shown in Fig. 9b–d, the X-ray images using P, O and Ca show corresponding images of the isolated scar. This shows that a Ca–PO_4 compound may be formed on the isolated wear scar during wear, which is likely to be generated from reaction with the ingredients of the lubricant (i.e., Hanks solution). This finding confirms that there exist tribochemical reactions at the MOM surfaces in Hanks solution. These reaction layers subsequently separate the surfaces and thereby hinder direct metal-on-metal contact. Thus it is found that under the present wear conditions, the wear behavior of like-on-like pairing of the CoCr alloy could be mitigated by the tribochemical reactions that produce a Ca–PO_4 compound – not yet verified – on the wear surfaces.

In addition, on the wear surface of cast CoCr (Fig. 9a), a number of quasi-cleavage fractured steps, possibly formed during formation of the wear debris, are observed, suggesting that wear mechanisms are involved in surface fatigue as well as abrasive wear. The wear surface of forged CoCr surrounding the isolated wear scar similar to that in Fig. 9, is shown in Fig. 10. As can be seen, almost no quasi-cleavage fractured steps similar to those observed on the surface of cast CoCr are found on the surface of forged CoCr, though there are scratches. Therefore, these observations may suggest that the forged CoCr is more resistant to surface fatigue wear than the cast CoCr, because the forged CoCr is more prone to transform martensitically and exhibits higher strength than the cast CoCr.

3.2.5. Changes in hardness after wear tests

Table 2 gives the Vickers hardness of the as-polished surface (before wear test, Hv(B.W.)) and the worn surface (after wear test on wear scar, Hv(A.W.)). The differences between the two hardnesses for each alloy, $\Delta Hv = Hv(A.W.) - Hv(B.W.)$ are also included in the table. It is clearly shown that the hardness of the cast CoCr alloy increased from 429 before the wear test to 450 afterwards, which gives $\Delta Hv = 21$, whereas that of the forged CoCr alloy increased from 374 to 438, giving $\Delta Hv = 64$. Accordingly, the increment of the hardness after wear is revealed to be larger in the forged CoCr alloy than in the cast CoCr alloy. This is due to the difference in work hardening rate between the two alloys. As already shown by the XRD analyses described in Section 3.1 (Fig. 3), the forged CoCr alloy can undergo SIMT more easily than the cast CoCr alloy, because SIMT becomes more likely to occur with decreasing carbon content (the stacking fault energy decreases with decreasing carbon content) [15]. In fact, the microstructure of the worn surfaces of the forged CoCr alloy almost completely evolved from the γ to the ε phase, a more stable and possibly stronger and more wear resistant crystallographic structure. Thus it can be deduced that the hardness of the cast CoCr mostly results from carbides precipitating in the matrix but not from the matrix itself, while the matrix of the forged CoCr exhibits higher strength than that of the cast CoCr alloy.

3.2.6. Wear mechanisms

According to Wimmer et al. [16], there are four major wear mechanisms governing the wear behavior of alloy systems: abrasion, surface fatigue, adhesion and tribochemical reactions. In the present study, with respect to wear appearance, we observed abrasion (Figs. 8–10). Although we omit detailed description of the surface fatigue wear, scars that may correspond to surface fatigue are found in Fig. 9a, as described in Section 3.2.4. Thus, as pointed out in a previous investigation [17], the wear caused by surface fatigue should not be ignored in the present tribosystem. In the Co–Cr–Mo alloy system studied here, wear caused by adhesion would not be the major mechanism of overall wear, as already stated in Section 3.2.3, because a considerably stable oxide film readily forms on the surface of the CoCr alloy, inhibiting direct contact between metal and metal, resulting in only a minor contribution to overall wear. Tribochemical reaction is also observed in the present tribosystem, as described in Section 3.2.4 and illustrated in Figs. 9 and 10. In the present case, the tribochemical reaction works as a wear-mitigating mechanism rather than the wear-accelerating one.

It is well documented in the literature [18] that abrasion is an often reported mechanism in MOM and other hip joint bearings, because scratches and grooves are always obvious. Abrasion may be induced by foreign particles or, more likely, from system-inherent particles such as fractured carbides, compressed wear debris and plastically deformed parts of the metal matrix. Furthermore, considering the appearance of wear in the present case, it is evident that the major wear mechanism is abrasion wear. The cast CoCr alloy, which contains a high percentage of carbon, predominantly experiences abrasion wear caused by torn-off carbide particles as well as carbide asperities, including the system-inherent particles mainly responsible for wear in the forged CoCr alloy which does not contain carbides. Such carbide-mediated abrasive wear is activated in the carbide-containing CoCr alloy, not in the carbide-free CoCr alloy. This is a cause of the higher wear loss actually observed in the present cast CoCr alloy. Thus it can be concluded that carbides precipitating in the matrix

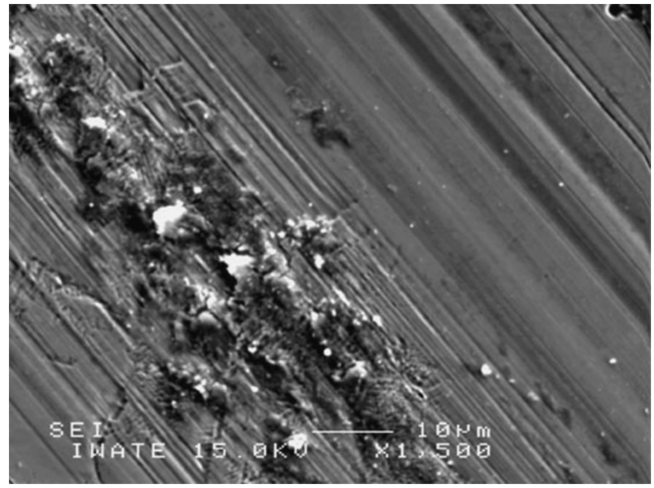

Fig. 10. SEM micrograph of the wear surface surrounding the isolated wear scar of the forged CoCr alloy. Note that there are no quasi-cleavage fractured steps (except for scratches on the surface), in contrast to those observed in the cast CoCr alloy, as shown in Fig. 9a.

of CoCr alloy are responsible for high MOM abrasive wear rates. However, prior to a definite conclusion on the role of carbides in the wear behavior of MOM bearings, more

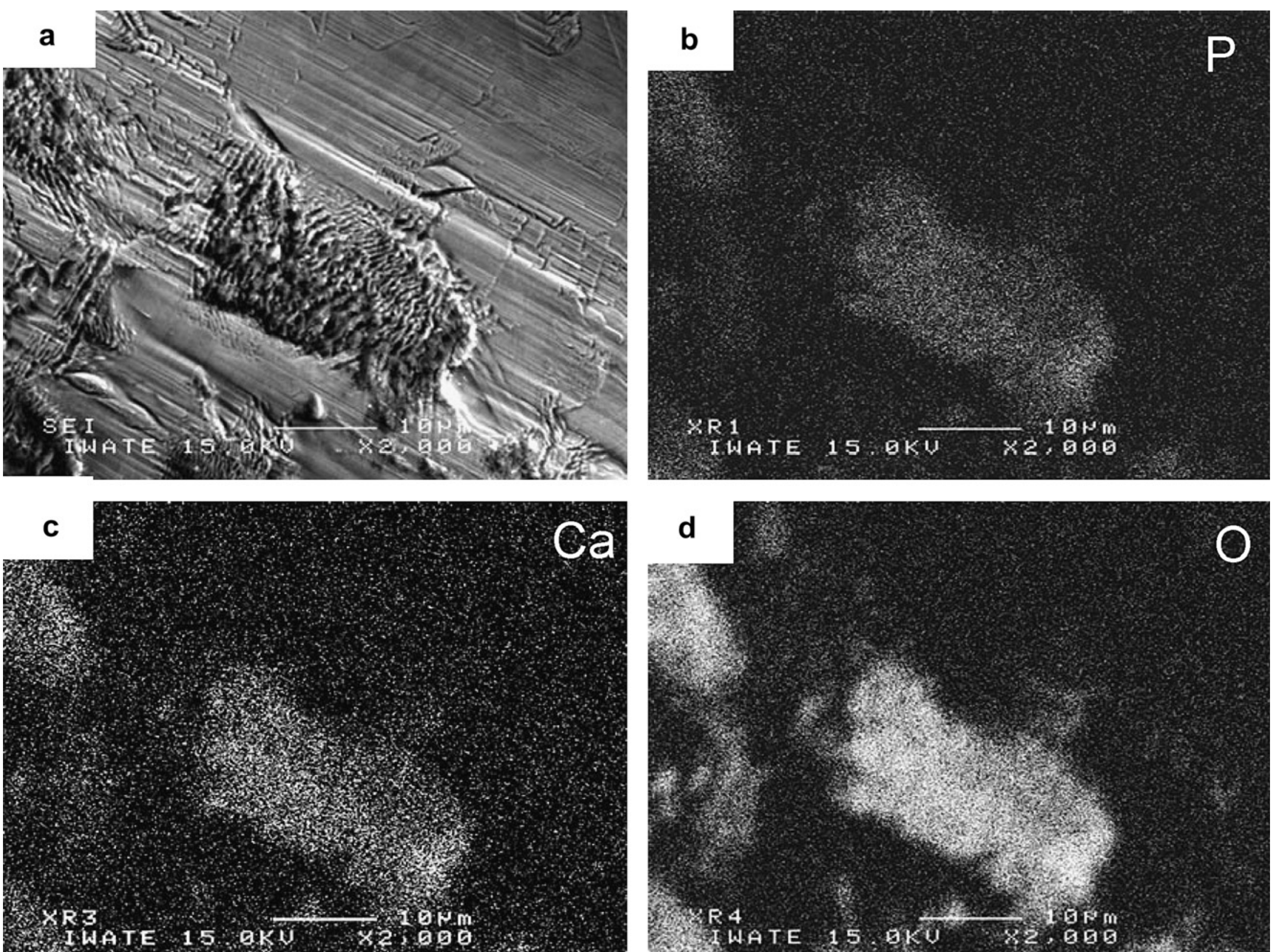

Fig. 9. Isolated wear scar on the wear surfaces of the cast CoCr alloy: (a) SEM micrograph obtained in secondary electron mode (SEI) and the X-ray maps of (b) P, (c) Ca and (d) O.

Table 2
Vickers hardness before and after wear tests of cast and forged CoCr alloys

Alloy	Hardness		
	Before wear test Hv(B.W.)	After wear test Hv(A.W.)	ΔHv = Hv(A.W.) − Hv(B.W.)
Cast CoCr	429	450	21
Forged CoCr	374	438	64

detailed studies on size, distribution and morphology of carbide precipitation are required.

Furthermore, we have to pay attention to the effect of SIMT on wear behavior. As described in Section 3.2.4, quasi-cleavage fractured steps actually observed on the wear surfaces of the cast CoCr would be indicative of surface fatigue wear. Such steps do not appear in the wear surfaces of the forged CoCr alloy (Fig. 10) which is prone to SIMT. Thus it can be deduced from this that a CoCr alloy without strengthening by carbides is more resistant to surface fatigue wear than one strengthened by carbides. In addition, as recently demonstrated by Büscher et al. [17,19], a nanocrystalline layer is generated just beneath the surface during wear. They considered from the findings that the prevailing wear mechanism in MOM bearings may not be abrasion, but surface fatigue within the recrystallized nanocrystalline layer, though it is not clearly understood how wear loss caused by the surface fatigue depends on the nanocrystalline structure layer. In the present authors' view, the nanocrystallized microstructures can be produced even in a bulk after heavily plastic deformation, mainly in fcc alloys if the alloy has much lower stacking fault energy. In fact, it was reported that, in austenitic stainless steel [20,21] and Co-based alloy with very low stacking fault energy [22], grain refinement occurs by a heavily plastic deformation process, involving formation of planar dislocation arrays, twins or martensites by SIMT in deformed grains. Thus it is deduced that an alloy more prone to SIMT exhibits a higher tendency to generate a nanocrystalline layer during the wear process. If this is the case, it is likely that the wear loss especially caused by surface fatigue depends on the trend of the SIMT, possibly governed by carbon content. However, at present there is limited information available regarding the effect of the nanocrystalline surface layer on wear behavior. Further studies are needed to establish the role of SIMT in the wear mechanisms of CoCr alloy in view of the surface fatigue wear.

Finally, the grain-size effect on the wear rate as well as the carbon effect have to be considered for elucidating the overall wear behavior of the CoCr alloy. In the present study the average grain size for the forged CoCr alloy was 11 μm, while that for the cast CoCr alloys was ~400 μm (but never precisely defined because of the dendritic structure). Since grain refinement as well as SIMT can affect generation of the nanocrystalline layer, the effect of grain refinement on surface fatigue wear should be considered for elucidating the overall wear mechanisms. Thus future work is required to reveal the grain-size effect on surface fatigue wear behavior.

4. Conclusions

1. The microstructure of the MOM wear surfaces of the forged CoCr alloy evolves from the γ to the ε phase during wear tests, in contrast to the cast CoCr alloy, which largely maintains the original γ phase.
2. Effective hardening of the wear surfaces during wear for the high carbon containing CoCr alloy cannot be obtained, because the presence of carbon increases the stacking fault energy, thereby eliminating SIMT.
3. The overall friction coefficient μ for MOM pairing of the forged CoCr alloy is slightly higher than that for the cast CoCr alloy.
4. Wear loss is more pronounced in the cast CoCr alloy than in the forged CoCr alloy, because carbide-mediated abrasive wear is activated in the carbide-containing CoCr alloy, but not in the carbide-free CoCr alloy. In addition, the wear loss resulting from surface fatigue, possibly depending on the trend of SIMT, should not be ignored.
5. A CoCr alloy without strengthening by carbides is more resistant to surface fatigue wear than one strengthened by carbides. The effect of grain refinement on surface fatigue wear should be considered in order to establish the overall wear loss mechanism.

Acknowledgements

The authors thank Mr. S. Fujinuma for technical assistance. Thanks are due to Ms. A. Ueyama for her help with operating the electron microscope. This research was supported by the Cooperation of Innovative Technology and Advanced Research in Evolutional Area of the Ministry of Education, Science and Culture of Japan.

References

[1] Chiba A, Li XG, Kim MS. Philos Mag A 1999;79:1533.
[2] Chiba A, Kim MS. Mater Trans 2001;42:2112.
[3] Chiba A, Kumagai K, Takeda H, Nomura N. Mater Sci Forum 2005;475–479:2317.
[4] Hiromoto S, Onodera E, Chiba A, Asami K, Hanawa T. Biomaterials 2005;26:4912.
[5] WIllert HG, Bertram H, Buchhorn GH. Clin Orthop 1990;258:95.
[6] Muratoglu OK, Bragdon CR, O'Connor DO, Jasty M, Harris WH. J Arthrop 2001;16:149.
[7] Amstutz HC, Campbell P, McKellop H, Schmalzreid TP, Gillespie WJ, Howie D, et al. Clin Orthop 1996;329(Suppl):S297.
[8] Sauer WL, Anthony ME. Predicting the clinical wear performance of orthopaedic bearing surfaces. In: Jacobs JJ, Craig TL, editors. Alternative bearing surfaces in total joint replacement. West Conshohocken (PA): American Society for Testing and Materials; 1998. p. 1–29.
[9] Medley John B, Chan Frank W, Krygier Jan J, Dennis Bobyn J. Clin Orthop 1996;329S:148.

[10] Chan FW, Bobyn DJ, Medley JB, Krygier JJ, Yue S, Tanzer M. Clin Orthop 1996;333:96.
[11] Tipper JL, Firkins PJ, Ingham E, Fisher J, Stone MH, Farrar R. J Mater Sci: Mater Med 1999;10:353.
[12] John KRS, Zardiacckas LD, Poggie RA. J Biomed Mater Res Part B: Appl Biomater 2004;68B:1.
[13] Kumagai K, Nomura N, Ono T, Hotta M, Chiba A. Mater Trans 2005;46:1578.
[14] Sage M, Guillaud CH. Rev Metall 1950;49:139.
[15] Beltran AD. Cobalt-base alloys. In: Sims CT, Stoloff NS, Hagel WC, editors. Superalloys. Chichester: Wiley; 1987. p. 35–163.
[16] Wimmer MA, Loos J, Nassutt R, Heitkemper M, Fischer A. Wear 2001;250:129.
[17] Büscher R, Täger G, Dudzinski W, Gleising B, Wimmer MA, Fischer A. Biomed Mater Res Part B: Appl Biomater 2005;72B:206.
[18] Sieber HP, Rieker CB, Kottig P. J Bone Joint Surg Br 1999;81:46.
[19] Büscher R, Fischer A. Wear 2005;259:887.
[20] Zhang HW, Hei ZK, Liu G, Lu J, Lu K. Acta Mater 2003;51:1871.
[21] Rigney DA, Fu XY, Hammerberg JE, Holian BL, Falk ML. Examples of structural evolution during sliding and shear of ductile materials. Scripta Mater 2003;49:977.
[22] Wu X, Tao N, Hong Y, Liu G, Xu B, Lu J, et al. Acta Mater 2005;53:681.